Soft Matter

PAPER

View Article Online
View Journal

Cite this: DOI: 10.1039/c4sm02374a

Striped patterns induced by delamination of drying colloidal films

F. Giorgiutti-Dauphiné* and L. Pauchard

Received 28th October 2014
Accepted 17th December 2014

DOI: 10.1039/c4sm02374a

www.rsc.org/softmatter

The drying of a dispersion of nanoparticles on a solid substrate can result in the formation of spontaneous well-ordered stripe patterns left on the substrate. The evaporation of solvent yields large stresses in the material which usually cause crack formation and delamination from the substrate. The formation of these stripes results from a balance between the drying stress which drives the delamination crack front propagation and the cohesive properties of the material. These solid residues arise behind the crack front and can be perpendicular or parallel to the front. It is then possible to inhibit these structures by modifying the cohesive properties of the material. This self-assembly into an ordered pattern can offer an efficient method to produce a patterned surface in a simple way.

1 Introduction

In recent years, there has been a great deal of interest in surface patterning, since it has the potential to achieve structures for a wide variety of applications: templates for microelectronics, optoelectronics or microfluidic devices[1–5] or arrays of magnetic nanoparticles.[6] Because of their importance in numerous applications, especially in the industry of coating, the case of planar films has motivated many studies. Dispersions of nanoparticles (colloids, polymers, DNA…) self-assemble into a multitude of ordered structures upon drying. In this way, various methods have been adopted for structuring particles on a flat substrate, including controlled evaporative self-assembly. In the case of a sessile colloidal droplet on a rigid substrate, an outward flow generated inside an evaporating drop drags the particles towards the contact line. Particles are left behind and form a ring stain. When the contact line is pinned during evaporation, solute particles generally accumulate in a ring around the periphery of the drop due to the "coffee ring effect".[7,8] The deposition of particles in ordered structures arises from the competition between the contact line pinning and the dewetting process. In some cases, the receded contact line exhibits a stick-slip motion which can induce some particular patterns exhibiting well-ordered wavelength.[9,10] The resulting morphologies mainly depend on particle concentration, particle size, and particle–substrate or particle–solvent interactions. Other self-assembly patterns are observed in the geometry of a dip-coating process.[11] In this case, the contact line breaks up into aggregates of nanoparticles to yield the formation of aligned stripe patterns perpendicular to the contact line.[12]

Here, we report a novel yet simple method to deposit aligned stripes on substrates by the natural drying of colloidal films. During the evaporation and solidification of the films, unless they are extremely thin, large stresses develop.[13] When these stresses exceed the strength of the material, crack patterns occur whose characteristic features depend on the mechanical properties of the material.[14–17] In particular, during the delamination process, a fingering instability occurs at the delamination crack front. This results in well-ordered solid stripes left on the substrate (Fig. 1c). Such stripe patterns are observed in various colloidal, mineral or organic systems and ferro-fluids. The study deals mainly with dispersions of silica particles. From experimental results, we deduce a deposition rate for particles which can be detached from the colloidal system to be deposited on the substrate to form solid stripes. The strong influence of the cohesive strength of the gelled film is evidenced and supported by indentation tests.

2 Experimental

2.1 Materials

Five different types of particulate materials were used: concentrated aqueous dispersions of silica particles (Ludox HS-40, SM-30, TM-50 purchased from Sigma-Aldrich) and nanolatex particles (provided by Rhodia Recherche, Aubervilliers, France); HS-40 was used in most experiments. These dispersions are stable in the absence of evaporation. The values of the surface tension $\gamma_{air/water}$ of the dispersions were measured by the Wilhelmy plate method and range in 57–67 mN m^{-1}. The initial viscosity η of the dispersion ranges from 3 to 6 mPa s (measurements using a rheometer Contraves LS30). For each dispersion, the weak polydispersity of the particles prevents them from crystallization (polydispersity $\sim$ 0.18). In the case of the silica sol, the stability of the dispersion is governed by the

CNRS, UMR 7608, Lab FAST, Bat 502, Campus Univ, F-91405, Orsay, France. E-mail: fred@fast.u-psud.fr; Fax: +33 1 69 15 80 60; Tel: +33 1 69 15 80 49

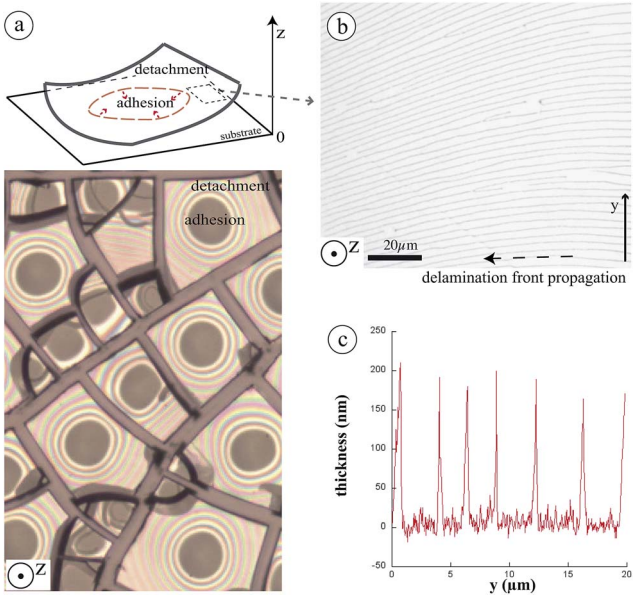

Fig. 1 (a) Partial delamination of fragments of a drying colloidal film of thickness h (image by optical microscopy in transmitted light, image height = 1.5 mm). Since fragments are transparent circular optical interference fringes display an air gap between the detached film and the substrate, and encircle adhering regions (dark circular regions); the resulting curled shape is shown in the sketch. (b) Stripe pattern left on the substrate after the propagation of a delamination front in the direction of the arrow (mean spacing between lines is $\bar{\lambda} = 3$ μm $\ll h = 100$ μm). (c) Typical cross-sectional analysis yielded the width and height of the above stripes (analysis from the AFM image).

interparticle colloidal interaction (Derjaguin–Landau–Verwey–Overbeek[18,19]). In the case of the nanolatex, particles are made of polystyrene, stabilized by the presence of surfactants (SDS); since the glass transition temperature of the particles is around 100 °oC, the particles are assumed to be rigid (not deformable) at room temperature. The main properties of these dispersions are reported in Table 1.

In order to study the effect of addition of polymer content to Ludox HS-40 dispersion, we use polyethylene oxide (PEO) purchased from Sigma-Aldrich. Indeed, a high affinity for silica surfaces is known for PEO resulting in an adsorption at high coverage.[20] The molecular weight of the polymer is 600 daltons. Polymers are dissolved in pure water at pH 9.5. This solution, with a weight concentration of polymers denoted as C_p, is used for the dilution of HS-40. As a result, the final polymer concentration in the HS-40 dispersion is $C_p/4$.

2.2 Methods

A quantity of the dispersion is deposited in a shallow and circular container (wall in Altuglass, diameter ∼ 30 mm, and height ∼ 5 mm) and left to dry from the free surface. The substrate is a non-porous glass plate, carefully cleaned with pure water and then with ethanol before being dried in a heat chamber at 100 °C. The contact line of the dispersion is quenched at the upper edge of the wall and remains pinned all along the drying process. At the final stage a film of approximately constant thickness is obtained in the center of the container. In this region, covering about 70% of the total surface area, the evaporation is uniform. The thickness h of the porous film is controlled by the initial volume of dispersion deposited in the container.

Table 1 Main characteristics of the samples considered in the experiments. Particle diameter: $2a$, solid weight fraction ϕ_m (data given by the manufacturer Grace Davison), and solid–liquid interfacial energy γ_{SL} (measurements using the indentation test just after the crack formation)

	$2a$ (nm)	ϕ_m	γ_{SL} (J m^{-2})
Nanolatex PS	25	0.30	0.07
Ludox HS-40	15	0.40	
Ludox SM-30	7	0.30	
Ludox TM-50	22	0.50	0.11
Maghemite	10	0.20	

The mechanical properties of materials can be approached by the instantaneous response of an applied force; in this way measurements of the fracture toughness were investigated using the indentation test (CSM Instruments Micro Indentation testing, MHT), with a four-sided Vickers indenter tip (pyramid-shaped diamond). The indenter, initially in contact with the surface of the solid film, is driven in the material up to a maximal load $F_{max} = 100$ mN, with a loading speed 100 mN min^{-1}. For sufficiently large indentation loads, applied to brittle materials, radial cracks emerge from the edges of the indenter (see Fig. 5). The same behaviours are obtained with $F_{max} = 200$ mN load.

3 Results

Starting from a film of a colloidal dispersion, the solvent loss concentrates the dispersion as particles approach each other. This results in a gel phase or close-packed solid. Since the pores of the material are filled with water, further evaporation causes the liquid menisci at the top layer of the particle array to generate compressive capillary stress, and consequently tensile stress in the plane of the film, since the substrate prevents the film from shrinking. When the tensile stress reaches a threshold value, successive cracks divide the solid film into sided domains resulting in the typical pattern shown in Fig. 1a. Since the film still dries from only one side, the porous network is compressed more on the drying face: a moment M results in an out-of-plane deformation of the film (Fig. 2a). Consequently the fragment becomes concave toward the drying side, with a characteristic curvature R^{-1} that is time-dependent. Indeed, the curvature of a warping plate increases rapidly with the evaporation rate V_E as predicted by a simple scaling law for the warping of a plate:[21,22] $R^{-1} \sim \frac{V_E}{h^2} t$ (Fig. 2b). This deformation drives the propagation of the delamination crack front that separates the adhering region from the detached one (Fig. 2c). During the delamination process the crack front usually destabilizes into a finger-like front (Fig. 3). This leaves periodic

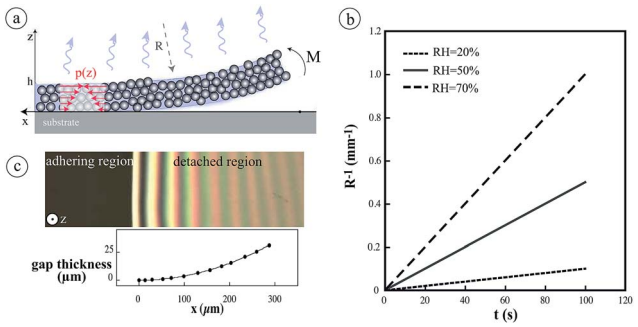

Fig. 2 (a) Sketch of the side view of the delamination of a drying film induced by differential stress (liquid pressure $p(z)$ in the pores). The moment M results in an out-of-plane displacement of the film. (b) Theoretical curvature as a function of time for warping plates dried at different relative humidities RH (plates thickness is ~100 μm). (c) Top view of the image, by optical microscopy, showing interference fringes close to the delamination crack front as a result of an air gap between the transparent film and the substrate.

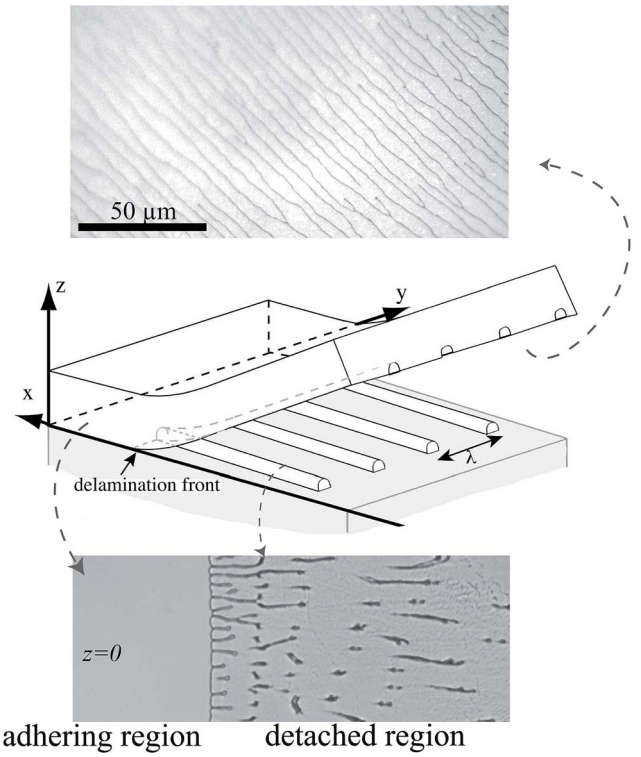

Fig. 3 Sketch showing the formation of stripes left on the substrate behind the delamination crack front: the delamination front propagates along the x-axis. Above: backside of a delaminated fragment showing the negative dimpled stripes. Bottom: image of the stripe formation behind the destabilizing crack front.

stripes made of particles on the substrate; stripes are normal to the delamination crack front, as shown in Fig. 1b.

Analysis from atomic force microscopy reveals the typical dimensions of these stripes (Fig. 1c): mean width = 0.8 μm, mean height = 175 nm which is lower than the film thickness h, and the characteristic distance between adjacent stripes $\lambda = 3$ μm. A consequence of the deposition of particles on the substrate is the formation of negative dimpled stripes at the backside of delaminated fragments (Fig. 3). Note that the size of the striped pattern is reproducible for a given system. The height of the lines of deposited particles can be roughly estimated using the following considerations. In general a crack advances only if the stress intensity factor K reaches the fracture toughness K_c that represents the material resistance to fracture. Assuming that the material is linear elastic, $K \sim \sigma\sqrt{H}$, where σ is the mechanical stress in the film and H is a length scale of the opening crack, and $K_c = \sqrt{\Gamma E}$, where E is the Young's modulus of the film and Γ is equal to the work used to create the new crack surfaces, work of adhesion in the case of an interfacial crack (assuming adhesion is due to the meniscus around each colloidal particle, $\Gamma \sim 10^{-2}$ J m^{-2}). The maximum value of the interfacial crack opening, H_m, corresponds to the maximum value of the stress, σ_m, in the film, close to the capillary pressure, P_{cap}, as $H_m \sim \dfrac{\Gamma E}{(-P_{cap})^2} = \dfrac{10^{-2} \times 10^9}{(-10^7)^2} \sim 1$ μm. H_m gives an order of magnitude of the height of the lines of deposited particles and is in agreement with the height measured by AFM (image in Fig. 1c).

The well ordered pattern results from the well-known hydrodynamic instability, *i.e.*, the Saffman–Taylor instability for viscous fluids.[23] This instability usually occurs at the interface between two viscous and immiscible fluids when the less viscous one invades the more viscous one. In our case, the interface moves with v_f, the delamination crack front velocity, and separates two immiscible fluids, air and the concentrated dispersion. Thus, the wavelength λ of the finger-like front which is the most amplified can be expressed as $\lambda \sim \xi\sqrt{\dfrac{\gamma_{air/water}}{\eta v_f}}$, where ξ is a length scale where the debonding occurs.[24] The range of action of the debonding process is the meniscus around each colloidal particle, so we estimate ξ equal to a fraction of the particle size. It is found that $\lambda \sim 10^{-9}\sqrt{\dfrac{70 \times 10^{-3}}{10^{-3} \times 3 \times 10^{-6}}} \sim 4$ μm, in agreement with the length scale measured in our systems. The expression for λ proposed is proportional to the particles size and inversely proportional to the front velocity. As the front velocity increases with the particles size, a change in the particle size implies no significant variations for λ. Thus, the measurements of λ are the same in the images of Fig. 5: 7 ± 1 μm (Fig. 5b), 6 ± 1 μm (Fig. 5c), 8 ± 1 μm (Fig. 5d, for stripes perpendicular to the front). Nevertheless, the particles size plays a significant role in the front velocity, and in the rigidity of the material, as evidenced by the results using the indentation test. This last point could be quantified by the following expression:[25]

$$E \propto \phi^4 \left(\frac{{E_0}^2 \gamma}{a}\right)^{1/3}$$

with E_0 and E being the elastic moduli of respectively a single particle and of the system. γ is the surface energy of the particle and a is the radius of the particle. Thus with small particles (SM-30), the system is more rigid, and no stripe

patterns are observed because the cohesion force is higher than the capillary pressure. One can note that the viscosity of the solvent can be modified using a cosolvent such as glycerol exhibiting high miscibility with water. However addition of a concentration greater than 10% to a dispersion results in a crack free coating. This concentration range is not sufficient to affect significantly the wavelength of the finger-like front.[26] The formation of the solid stripes requires first the destabilisation of the delaminated crack front to form a finger-like front, and then particles have to be expelled from the cohesive gel to form settling aggregates on the substrate. These aggregates account for nucleation centers to collect more particles as the delamination crack front advances to finally form the residues (inset in Fig. 4b). Strong forces are required to expel particles from the cohesive gel (Fig. 2c). This is achieved in the small opening angle between the film and the substrate, close to the delamination crack front. Indeed, in this confined area, an interface between the liquid meniscus and air is subjected to large capillary pressure due to the large curvature of the interface. This large capillary pressure possibly overcomes the cohesion of the material, and consequently restructures the colloidal packing.

As a result, a fraction ϕ_d of particles in the water-supported film can be detached from the colloidal packing and then could be deposited onto the substrate. The deposition process results from the competition between the speed of the delamination crack front v_f and the particle deposition rate v_d, similar to the competition between a liquid contact line velocity and the particle deposition rate studied by Yang *et al.*[27] The deposition rate v_d depends mainly on the volume fraction of particles ϕ_d available to deposit onto the substrate, and on the evaporation rate as $v_d \propto \phi_d V_E$, for $\phi_d \ll 1$, where the proportionality coefficient depends on the particle–particle and particle–substrate interactions.[28] Assuming the quantity ϕ_d to be constant during the delamination process, the deposition rate v_d is kept constant, for the given drying conditions. Thus, one can define a criterion for the formation of the solid stripes: for $v_f > v_d$, particles have not sufficient time to deposit onto the substrate, no residue is left on the substrate, while the condition $v_f < v_d$ indicates the formation of the stripes. The experimental results reported in Fig. 4 provide estimation for v_d. The data in Fig. 4a concern measurements of the speed of the delamination crack front for different drying conditions and for one system (silica films HS-40). In general, when the debond length exceeds several times the film thickness, the delamination crack front velocity decreases up to a roughly constant value (a typical value of the velocity v_f is then a few μm s^{-1}, greater than the evaporation rate $= 5 \times 10^{-8}$ m s^{-1}), till fingering instability occurs. The red dots in the graph correspond to the appearance of the first residue. The corresponding velocity v_f represents the critical velocity by which the particles are deposited onto the substrate, that is v_d. The experiments reveal weak influence of the relative humidity on the values of v_d (roughly 1 μm s^{-1} for the RH range between 20 and 70% in Fig. 4a). This can be understood as the wet debond front is a very confined area where evaporation is very low. The values of v_d deduced from Fig. 4a range between 2 and 5 μm s^{-1}, which is in agreement with calculated deposition speeds for diluted particle suspensions close to 5% in ref. 28.

We report in Fig. 4b the formation of a stripe pattern for different colloidal systems, keeping the drying conditions constant; results are reported in Table 1 for colloidal gels of silica particles (SM-30, HS-40 and TM-50) and organic particles (nanolatex). In particular particle size and particle charge of the colloidal film affect the occurrence of the fingering instability, also the stripe pattern. The deposition rate v_d is higher for TM-50 than for HS-40, whereas for silica particle SM-30, no stripe patterns are formed. These results highlight the role of the cohesion of the system in the formation of the stripes. v_d depends on the size of the particles as it stands for the velocity required for a particle to move to a distance close to its diameter. Moreover, for too smallest particles (silica particle SM-30), the capillary forces cannot overcome the cohesive strength of the material. Thus the resulting volume fraction of particles ϕ_d available to deposit onto the substrate is larger for TM-50 than for HS-40 and close to 0 for SM-30. For gels made of nanolatex particles, the stripe pattern is more complex due to two modes of propagation of the delamination crack front: fingering instability resulting in stripes perpendicular to the delamination crack front, and stick-slip motion leading to stripes parallel to the front (Fig. 5d). These observations strongly suggest that the formation of the stripe patterns on a substrate depends on the physicochemical and mechanical properties of the delaminated gel.

Stripe patterns are strongly dependent on the fraction of particles available to deposit onto the substrate, and by the way, on the cohesive strength of the material. Indeed, due to the small opening angle between the film and the substrate, particles can be detached from the gel if the cohesive strength of the gel is low. On the contrary, we expect no stripe pattern on the substrate for films exhibiting high cohesive strength. A simple way to compare the cohesive strength of dried films is to observe

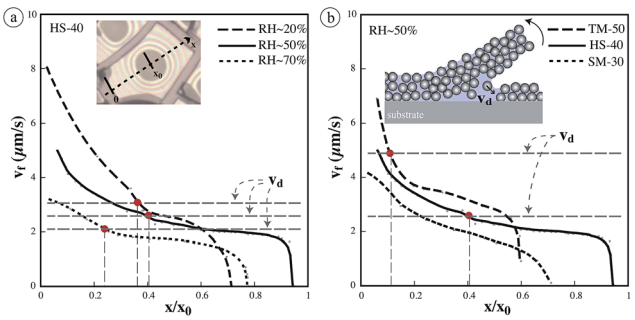

Fig. 4 Speed v_f of the delamination crack front along the x-axis ($x = 0$ corresponds to the fragment limit, and $x = x_0$ is located at the center of the circular adhering region) (a) for silica films (HS-40) dried at different relative humidities RH, and (b) for different silica films (TM-50, HS-40, SM-30) dried at RH ∼ 50%. Reduced speed causes the development of fingering instabilities, indicated by the red dot, resulting in the formation of the stripe pattern on the substrate. The deposition process can be approached by considering a mismatch between the speed of the crack front and a characteristic speed v_d of particle deposition (inset).

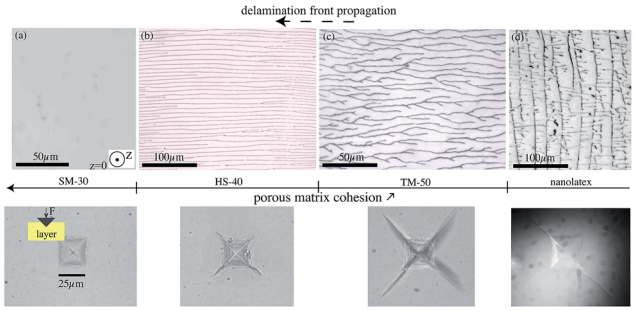

Fig. 5 Typical patterns at the surface of the substrate after the delamination process of different films: (a) deposition-free (SM-30), (b) stripe pattern (HS-40), (c) fork (TM-50), (d) stripe and ring patterns (nanolatex). Bottom: prints of indent for the different films: short or long radial cracks can nucleate from the indent, and are characteristic of the fracture toughness of the material.

the ability of materials to propagate crack or resist crack propagation by the indentation test (see the Experimental section). For sufficiently large indentation loads, radial cracks emerge from the edges of a Vickers indenter (see Fig. 5). Therefore, different dried films are compared in Fig. 5. Except for dried films of SM-30, indentation loads lead to radial cracks, and stripe patterns due to the delamination process: consequently films of SM-30 reveal a higher cohesive strength than the other studied films. For dried films exhibiting a high cohesive strength, no radial cracks due to the indentation load (SM-30) and no stripe pattern due to the delamination process are observed as is the case for films with lower cohesive strength (HS-40, TM-50, nanolatex). Note that, from the experimental results, the higher cohesive strength is typical of the gel made of small sized particles. It is then possible to prevent the formation of the well-ordered stripe pattern observed in HS-40 films, for example, by modifying the cohesive properties of the material. A way to do that is to increase the cohesive strength of the gel, by adding polymers; the internal bonding between particles is modified by adsorbing polymer chains (PEO) at the particle surface.[20] We have observed that the surface of the substrate is free of stripes after the film delamination process. This result confirms that a low cohesive strength is necessary to form stripe patterns during the delamination process.

4 Conclusion

A colloidal film of nanoparticles usually exhibits mechanical instabilities during drying resulting in crack formation and the delamination process. The delamination crack front can destabilize into a finger-like front. This leaves periodic solid stripes, perpendicular to the interfacial crack front. The potential application of this phenomenon could be the design of patterning substrates. For an effective process, the deposition area needs to be important compared to the total surface. We found from our experiments that the typical deposition area of stripe patterns is about 1/3 of the total surface of a fragment. Measurements by image processing show that residues cover 15% of the surface of the substrate. Capillary forces occurring in the confined area between the substrate and the film close to the delaminated front can overcome the cohesive strengths provided there are low enough. Experimental results evidence the role of the cohesive strength of different materials using the indentation test. In particular the modification (decrease) of the cohesive strength of a film by adsorbing polymer chains onto the colloidal particle surface inhibits the stripe patterns.

Acknowledgements

We thank Patrick Guenoun (LIONS-CEA) and Mokhtar Adda-Bedia (LPS-ENS) for useful discussions, Alban Aubertin, Lionel Auffray, Christian Borget, and Rafaël Pidoux (FAST-University Paris Sud) for engineering and technical support.

References

1 N. Tas, T. Sonnenberg, H. Jansen, R. Legtenberg and M. Elwenspoek, *J. Micromech. Microeng.*, 1996, **6**(4), 385–397.
2 C. Mastrangelo, *Tribol. Lett.*, 1997, **3**, 223–238.
3 C. Hui, A. Jagota, Y. Lin and E. Kramer, *Langmuir*, 2002, **18**(4), 1394–1407.
4 C. S. Davis and A. J. Crosby, *Soft Matter*, 2011, **7**, 5373–5381.
5 Y. Ebata, A. B. Croll and A. J. Crosby, *Soft Matter*, 2012, **8**, 9086–9091.
6 J. Shi, S. Gider, K. Babcock and D. D. Awschalom, *Science*, 1996, **271**, 937–941.
7 R. D. Deegan, O. Bakajin, T. F. Dupont, G. Huber, S. R. Nagel and T. A. Witten, *Nature*, 1997, **389**, 827–829.
8 R. Deegan, *Phys. Rev. E: Stat. Phys., Plasmas, Fluids, Relat. Interdiscip. Top.*, 2000, **61**, 475.
9 E. Adachi, A. S. Dimitrov and K. Nagayama, *Langmuir*, 1995, **11**, 1057–1060.
10 S. Maheshwari, L. Zhang, Y. Zhu and H.-C. Chang, *Phys. Rev. Lett.*, 2008, **100**, 044503.
11 J. Huang, F. Kim, A. Tao, S. Connor and P. Yang, *Nat. Mater.*, 2005, **4**, 896–900.
12 W. Han, B. Li and Z. Lin, *ACS Nano*, 2013, **7**, 6079–6085.
13 P. Xu, A. S. Mujumdar and B. Yu, *Drying Technol.*, 2009, **27**, 636–652.
14 J. W. Hutchinson and Z. Suo, *Adv. Appl. Mech.*, 1992, **29**, 63.
15 A. Groisman and E. Kaplan, *Europhys. Lett.*, 1994, **25**, 415–420.
16 L. Pauchard, *Europhys. Lett.*, 2006, **74**, 188.
17 V. Lazarus and L. Pauchard, *Soft Matter*, 2011, **7**, 2552–2559.
18 B. Derjaguin and L. Landau, *Acta Physicochim. URSS*, 1941, **14**, 633.
19 E. J. Verwey and J. T. G. Overbeek, *Theory of Stability of Lyophilic Colloids*, Elsevier, Amsterdam, 1948.
20 K. Wong, P. Lixon, F. Lafuma, P. Lindner, O. A. Charriol and B. Cabane, *J. Colloid Interface Sci.*, 1992, **153**, 55–72.
21 C. J. Brinker and G. W. Scherer, *Sol–Gel Science: The Physics and Chemistry of Sol–Gel Processing*, Elsevier Science, 1990.
22 F. Giorgiutti-Dauphiné and L. Pauchard, *Eur. Phys. J. E*, 2014, **37**, 39.

23 P. Saffman and G. Taylor, *Proc. R. Soc. London, Ser. A*, 1958, **245**, 312–329.
24 R. J. Fields and M. F. Ashby, *Philos. Mag.*, 1976, **33**, 33–48.
25 K. Kendall, N. M. Alford and J. D. Birchall, *Proc. R. Soc. London, Ser. A*, 1987, **412**, 269.
26 F. Boulogne, L. Pauchard and F. Giorgiutti-Dauphiné, *Soft Matter*, 2012, **8**, 8505.
27 X. Yang, C. Y. Li and Y. Sun, *Soft Matter*, 2014, **10**, 4458–4463.
28 B. Prevo and O. Velev, *Langmuir*, 2004, **20**, 2099–2107.

